ResearchGate

See discussions, stats, and author profiles for this publication at: https://www.researchgate.net/publication/317497214

Biogeochemical cycling of Fe and Fe stable isotopes in the Eastern Tropical South Pacific

Article *in* Marine Chemistry · June 2017

DOI: 10.1016/j.marchem.2017.06.003

CITATIONS
3

READS
109

10 authors, including:

Seth G John
University of Southern California
79 PUBLICATIONS **1,728** CITATIONS
SEE PROFILE

Thomas Weber
University of Rochester
21 PUBLICATIONS **424** CITATIONS
SEE PROFILE

Chris Marsay
University System of Georgia
32 PUBLICATIONS **801** CITATIONS
SEE PROFILE

Claire P. Till
Humboldt State University
16 PUBLICATIONS **56** CITATIONS
SEE PROFILE

Some of the authors of this publication are also working on these related projects:

marDOS project: sources and fate of marine dissolved organic sulfur (DOS) View project

Quantifying trace element and isotope fluxes at the ocean-sediment boundary View project

All content following this page was uploaded by Chris Marsay on 16 March 2018.

The user has requested enhancement of the downloaded file.

Marine Chemistry xxx (xxxx) xxx–xxx

Contents lists available at ScienceDirect

Marine Chemistry

journal homepage: www.elsevier.com/locate/marchem

Biogeochemical cycling of Fe and Fe stable isotopes in the Eastern Tropical South Pacific

Seth G. John[a,b,*], Joshua Helgoe[a], Emily Townsend[a], Tom Weber[c], Tim DeVries[d,e], Alessandro Tagliabue[f], Keith Moore[g], Phoebe Lam[h], Chris M. Marsay[a,i], Claire Till[j]

[a] Department of Earth and Ocean Sciences, University of South Carolina, Columbia, SC, United States
[b] Department of Earth Sciences, University of Southern California, Los Angeles, CA, United States
[c] Department of Earth and Environmental Science, University of Rochester, Rochester, NY 14627, United States
[d] Department of Geography, University of California, Santa Barbara, CA 93106, United States
[e] Earth Research Institute, University of California, Santa Barbara, CA 93106, United States
[f] Department of Earth, Ocean and Ecological Sciences, School of Environmental Sciences, University of Liverpool, Liverpool, UK
[g] Department of Earth System Science, University of California, Irvine, CA 92697, United States
[h] Department of Ocean Sciences, University of California, Santa Cruz, CA 95064, United States
[i] Skidaway Institute of Oceanography, University of Georgia, Savannah, GA, United States
[j] Chemistry Department, Humboldt State University, Arcata, CA 95521, United States

ABSTRACT

The basin-scale distributions of iron (Fe) and Fe isotopes provide important insights into the biogeochemical cycling of this growth-limiting micronutrient in the ocean. Here we present new observations of dissolved Fe concentrations and stable isotope ratios (δ^{56}Fe) from the US GEOTRACES Eastern Pacific Zonal Transect GP16. The western portion of the transect is characterized by low dissolved Fe concentrations with a heavy δ^{56}Fe signature of + 0.4 to + 0.6‰, similar to the dust-influenced North Atlantic deep waters. This is punctuated by Fe inputs from hydrothermal vents along the East Pacific Rise, with a δ^{56}Fe of − 0.3‰. One striking feature of the transect is a large plume of high dissolved Fe and low δ^{56}Fe (0 to − 0.5‰) in the east, near the Peru margin. Here, maximum dissolved Fe occurs between 1000 and 3000 m and the elevated concentrations persist over 1000 km from the margin. The region of markedly lower δ^{56}Fe extends even further, to roughly 4000 km offshore. The mid-slope depth at which this plume occurs (1000–3000 m) is at odds with current conceptual and numerical models of Fe inputs along continental margins, which predict a shallower and more restricted dissolved Fe maximum (upper-slope; ~100–1000 m). Here, we explore four possible explanations for the mid-slope Fe plume: (1) Fe fluxes are actually higher from mid-slope sediments; (2) the mid-slope plume is transported from a remote region (3) mid-slope Fe originates from resuspended sediments in a very persistent form, which remains in the dissolved phase for longer than Fe released from the upper-slope; (4) Fe is supplied from upper-slope sediments, and then transferred to greater depth by reversible scavenging onto sinking particles. Simple modeling is used to show that both input of persistent Fe from mid-slope sediments and reversible scavenging could explain the data. Flux of a more persistent chemical form of Fe from the mid-slope would be consistent with other tracers such as particle composition and ^{228}Ra, which suggest that lithogenic sediments are preferentially resuspended at this depth, but may be at odds with the low δ^{56}Fe signature. Reversible scavenging is consistent with both Fe concentrations and δ^{56}Fe. Whatever its provenance, the plume observed near the Peru margin impacts Fe concentrations and δ^{56}Fe throughout the entire eastern South Pacific region, suggesting that the roles of persistent Fe input and reversible scavenging should be appraised in fully coupled iron-carbon cycle models in order to better understand the global cycling of Fe and δ^{56}Fe.

1. Introduction

Iron is a globally important micronutrient that affects biological productivity and metabolism worldwide (Tagliabue et al., 2017; Moore and Doney, 2007; Boyd and Ellwood, 2010). The study of iron concentrations and iron stable isotope ratios (δ^{56}Fe) dissolved in seawater

* Corresponding author at: Department of Earth and Ocean Sciences, University of South Carolina, Columbia, SC, United States.
E-mail address: sethjohn@usc.edu (S.G. John).

http://dx.doi.org/10.1016/j.marchem.2017.06.003
Received 1 March 2017; Received in revised form 30 May 2017; Accepted 7 June 2017
0304-4203/ © 2017 Published by Elsevier B.V.

can elucidate the sources, sinks, and biogeochemical cycling of this important element in the world oceans (Conway and John, 2014). The US GEOTRACES GP16 cruise recently transected the Eastern Tropical South Pacific and observed two striking features that reveal subsurface sources of Fe in this basin: (i) a region of elevated Fe emanating from hydrothermal vents along the South East Pacific Rise (SEPR), and (ii) a region of elevated Fe along the Peruvian margin, which houses one of the largest oxygen minimum zones (OMZs) worldwide. Here we present complete transects of Fe concentrations and δ^{56}Fe from this cruise.

The hydrothermally-influenced western portion of the transect has already been reported and interpreted in previous work (Resing et al., 2015; Fitzsimmons et al., 2017). Dissolved and particulate Fe in the plume emanating from the SEPR extends thousands of kilometers westwards through the deep Pacific ocean (Resing et al., 2015), highlighting the importance of hydrothermal vents in supplying Fe to the deep ocean. Both the dissolved and particulate plumes sink subtly as they move westward, crossing isopycnals and departing downwards from the SEPR Mn and δ^{3}He plumes. Dissolved and particulate Fe in the hydrothermal plume have similar δ^{56}Fe (~ -0.3‰), suggesting that Fe in both size-classes occurs in the same chemical form, and that Fe exchanges between particulate and dissolved phases within the plume (Marsay et al., n.d.; Fitzsimmons et al., 2017).

Our paper focuses on the eastern section of the GP16 transect, where the intersection of the OMZ with the Peruvian margin leads to distinct Fe and δ^{56}Fe behavior. Reduced Fe(II) is water soluble, while oxidized Fe(III) quickly precipitates unless bound to an organic ligand. In this region, sediment porewater profiles in cores taken above ~700 m show high (μM) porewater Fe concentrations all the way up to the sediment-water interface, allowing for large fluxes of reduced Fe from the sediments at these depths (Heller et al., 2017; Noffke et al., 2012; Scholz et al., 2014a; Scholz et al., 2014b; Vedamati et al., 2014; Scholz et al., 2016). The input of isotopically light Fe(II) from anoxic porewaters leaves a characteristically low δ^{56}Fe signature in seawater (Severmann et al., 2010; John et al., 2012; Boiteau et al., 2013; Chever et al., 2015; Fitzsimmons et al., 2016). Previous analyses above the Peru shelf found dissolved δ^{56}Fe ranging from -0.31 to -1.25‰ (Chever et al., 2015), which is somewhat heavier than observed in benthic flux chambers and seawater overlying reducing sediments along the California Margin (-2 to -4‰) (Severmann et al., 2006; John et al., 2012). A heavier sedimentary dissolved δ^{56}Fe flux can be attributed to both extensive loss of reduced Fe from sediments, and to the precipitation of Fe sulfides, both of which have been previously observed in Peru Margin sediments (Scholz et al., 2014a; Scholz et al., 2014b). Here, we use our basin-scale observations of dissolved Fe and δ^{56}Fe to further explore the Fe source mechanisms along the Peruvian margin.

2. Methods

2.1. Chemical analyses

Water samples were collected as part of the US GEOTRACES GP16 transect using the sampling system described by Cutter and Bruland (2012). Samples were filtered through cleaned and flushed 0.2 μm Acropak-200 Supor capsule filters. Onshore, samples were analyzed for Fe concentrations and δ^{56}Fe according to published methods (Conway et al., 2013). Briefly, 1 L samples were acidified to pH 1.8 with 1 mL L^{-1} quartz-distilled HCl and left for at least two months to redissolve any Fe that may have precipitated onto bottle walls since sampling. Samples were amended with a ~1:1 ^{57}Fe-^{58}Fe double spike, and Fe was extracted onto Nobias chelating resin PA-1 at pH 2, then the pH adjusted to ~6. After separating the Nobias from seawater by filtration, Fe was released from the Nobias resin with 5% teflon-distilled HNO_3 and purified by anion exchange chromatography. Finally, samples were analyzed for [Fe] and δ^{56}Fe on a Neptune multi-collector ICPMS at the University of South Carolina, with δ^{56}Fe reported relative to IRMM-014.

Prior to processing large-volume samples, all samples were analyzed for [Fe] by using a similar procedure on 10 mL samples. All reagents were scaled down by a factor of 100. These 10 mL samples were prepared in 15 mL centrifuge tubes so that removal of the seawater, rinsing of the resin with ultrapure water, and extraction of the metals with 5% HNO_3 could be performed using a home-built procedure on the PrepFast sample processing robot (Elemental Scientific Incorporated). These values were used to determine the necessary double-spike concentration for the large-volume analysis and are generally not reported, except in rare cases where there was a problem with concentrations measured on large-volume samples. Accuracy and precision of both concentration and isotopic measurements is discussed at length in Conway et al.; measured concentrations of SAFe reference samples were within the community consensus ranges.

All data is available online through the Biological and Chemical Oceanography Data Management Office (BCO-DMO) and will be included in the 2017 GEOTRACES Intermediate Data Product.

2.2. Modeling

Several hypotheses about Fe biogeochemical cycling are explored using a coarse-resolution 3-dimensional ocean circulation inverse model (OCIM). This model represents the time-mean circulation at a horizontal resolution of 2° latitude and longitude with 24 vertical layers, and is optimized using the observed distributions of potential temperature, salinity, ^{14}C and CFCs, as well as climatological estimates of sea-surface height and sea-surface heat and freshwater fluxes (DeVries, 2014). We conducted a set of highly idealized model experiments to test whether various sedimentary Fe source patterns are consistent with the observed basin-scale distribution of dissolved Fe. Each experiment solves the following tracer conservation equation for the steady-state distribution of Fe:

$$\frac{d[Fe]}{dt} = \boldsymbol{A}[Fe] + S_{Fe} - L_{Fe} \quad (1)$$

where S_{Fe} is the idealized Fe source function, L_{Fe} is the loss of Fe, and $\boldsymbol{A}$ is the OCIM circulation model represented as a "transport matrix" (Khatiwala, 2007). This is far from a complete treatment of the ocean Fe cycle, which would need to consider multiple Fe sources (e.g. dust and hydrothermal vents) and realistic internal cycling processes (e.g. biological uptake, scavenging and colloidal aggregation, as well as remineralization and recycling), none of which are represented in our model. Instead, it is more appropriate to think of this exercise as an effort to understand the influence of different Fe sources, redistributed by a realistic three-dimensional circulation, on the large-scale distribution of dissolved Fe. Two different configurations of the model are used. In the first (source-only), we simply use the model to visualize how different sources of Fe are circulated through the basin, to ask whether the plume of Fe between 1000 and 3000 m near the Peru margin might simply reflect the pattern of Fe inputs. In the second (source-sink), we simulate mechanisms of Fe loss by reversible or irreversible scavenging onto sinking particles, to test whether the location of the plume might reflect a more complex balance between inputs, removal, and cycling of Fe.

2.2.1. Source-only configuration

While we make no attempt to resolve mechanisms of Fe loss in this model configuration, a sink of Fe is required to derive a steady-state solution to Eq. (1), allowing us to visualize the transport trajectory of different dissolved Fe sources. We therefore assume Fe is lost via simple first-order "decay" at rate k_{decay} following:

$$L_{Fe} = k_{decay} \cdot [Fe] \quad (2)$$

Mathematically, this is similar to very early models (e.g. Archer and Johnson, 2000), which included a first-order scavenging without considering the effect of particle concentration on scavenging rates, but we

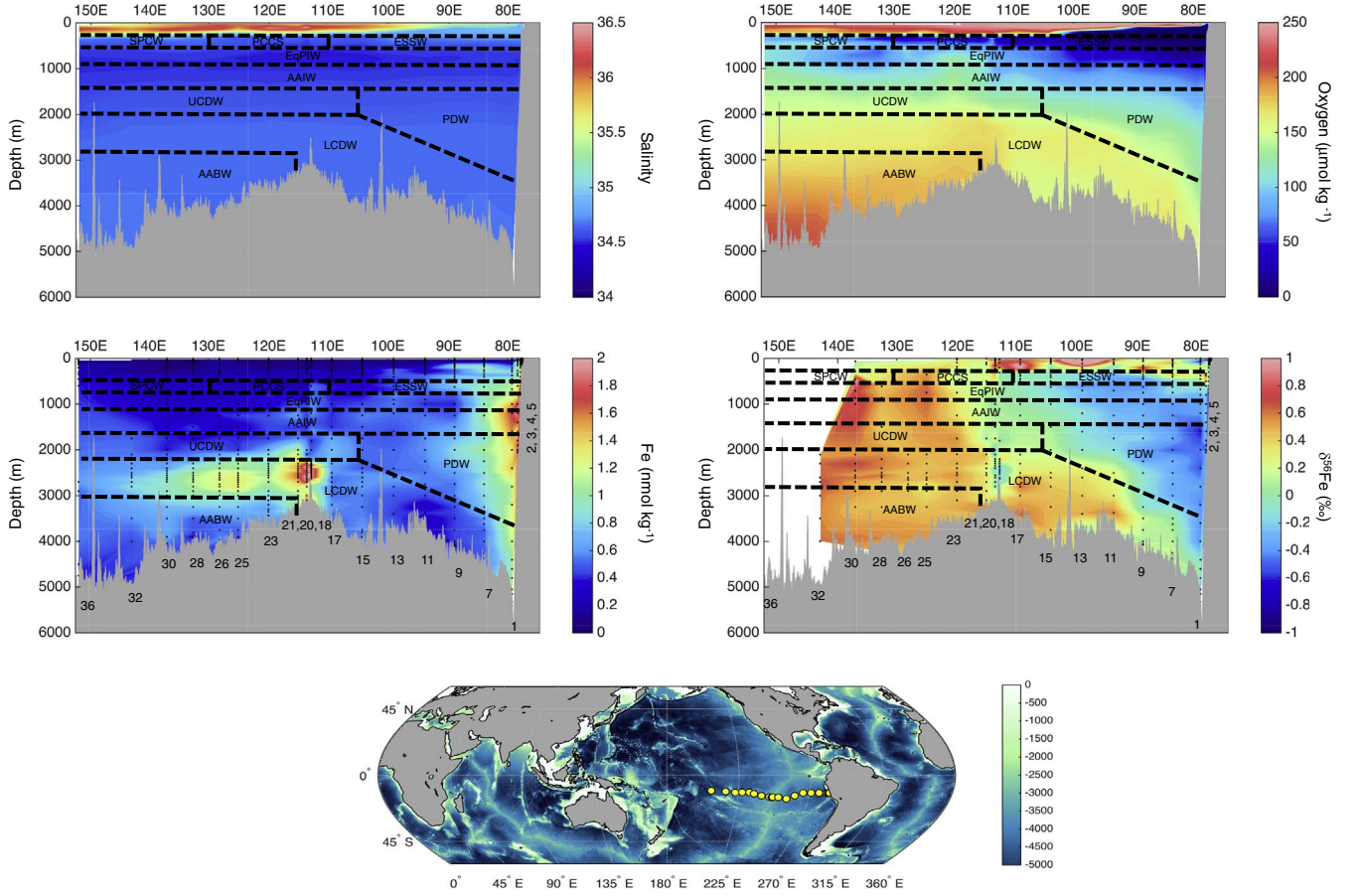

Fig. 1. Distribution of salinity, oxygen, Fe, and δ^{56}Fe along the GP16 transect. Points on the sections of Fe and δ^{56}Fe represent individual sampling bottles. Approximate locations of various water masses are drawn on based on the water mass analysis of Peters et al. (2017). Data is interpolated using a routine which first interpolates linearly between each point in vertical profiles, then interpolates horizontally between profiles.

do not consider this to be a mechanistic treatment of Fe loss. We choose a dissolved Fe half-life of 50 years (k_{decay} = 0.014 yr^{-1}), which is broadly consistent with other estimates of dissolved Fe lifetime in the deep ocean (Moore et al., 2004; Parekh et al., 2004; Tagliabue et al., 2014).

A total of four different "source functions" (S_{Fe}) of dissolved Fe were visualized using this method. First, a "regenerative" source of dissolved Fe was modeled, in which S_{Fe} was set proportional to the remineralization rate of organic P, assuming an arbitrary fixed Fe/P stoichiometry for all biological remineralization. Organic P remineralization was derived from previous biogeochemical simulations using this circulation model (DeVries et al., 2014). Second, a "reducing sediment" source was modeled, in which S_{Fe} was set proportional to the remineralization rate of organic P in seafloor sediments. This approach is similar to the parameterization in several current global Fe cycle models (Elrod et al., 2004; Tagliabue et al., 2016), except that we use P remineralization as a model proxy for organic carbon flux to the seafloor which the model does not explicitly track. Sedimentary organic P remineralization is taken from DeVries et al. (2014) who compensate for the low-resolution of the model grid by interpolating higher-resolution bathymetry. Third, a "generic sediment" source of Fe was modeled, in which S_{Fe} is proportional to the total sedimentary surface area, representing uniform input from oxic and anoxic sediments alike. This is motivated by recent observations from the North Atlantic that benthic fluxes from oxic are of similar magnitude to reducing sediments (Conway and John, 2014). Finally, we model a "slope sediment" source, in which S_{Fe} is proportional to sediment surface area where the ocean intersects basin margins, i.e. along the vertical interfaces between sediments and the ocean on the model grid. This aims to represent the preferential resuspension of sediments by internal wave action on steep slopes at basin edges (Cacchione and Drake, 1986).

2.2.2. Source-sink configuration

In this model configuration, we combine the "reducing sediment" source function (described above) with more realistic representations of dissolved Fe scavenging. Reducing sediments are the best understood benthic source of dissolved Fe, and are represented in most global models. Our goal here is therefore to test whether this source can reproduce the 1000–3000 m plume when combined with more complex removal and cycling processes.

Two scavenging parameterizations are tested. In the first, scavenging is assumed to be irreversible, with a rate controlled by the availability of particles to adsorb to:

$$L_{Fe} = k_{irreversible} \bullet [Fe] \bullet [POC] + k_{decay} \bullet [Fe] \quad (3)$$

Here, [POC] through the water column is taken from the model output of DeVries et al. (2014), and $k_{irreversible}$ (mM POC^{-1} nM Fe^{-1}) is the scavenging rate constant, which is varied to best match the observed dissolved Fe distribution. This parameterization aims to test the hypothesis that low scavenging rates between 1000 and 3000 m, due to scarcity of particles, might explain the dissolved Fe plume in this depth interval.

The second parameterization represents classical "reversible scavenging" (Bacon and Anderson, 1982), by explicitly simulating a particle-adsorbed fraction (Fe_{ads}) that remains in equilibrium with the surrounding seawater:

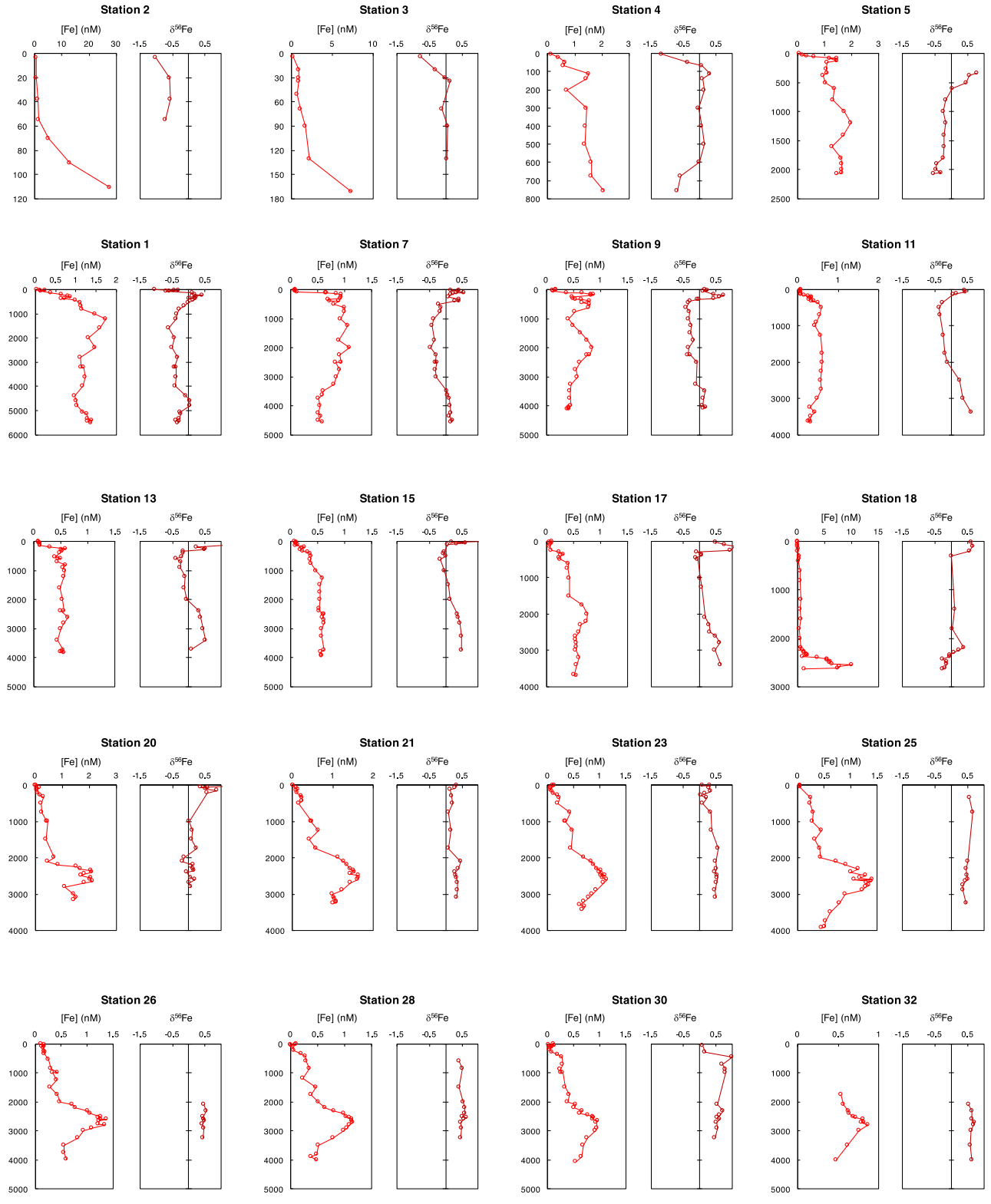

Fig. 2. Profiles of dissolved Fe concentrations and δ^{56}Fe for individual stations analyzed on the GP16 transect.

$$Fe_{ads} = \frac{K_d \bullet POC}{K_d \bullet POC + 1} Fe_{total} \quad (4)$$

Here Fe_{total} is the sum of dissolved and adsorbed Fe, and $K_{reversible}$ (mM POC^{-1}) is the partition coefficient for reversible binding of Fe onto POC, which is varied to best match observed dissolved Fe. The adsorbed fraction settles through the water column at a rate of 50 m/day, characteristic of sinking organic particles (Guidi et al., 2008), redistributing Fe through the water column but not removing it from the ocean as a whole. The ultimate sink of Fe from the ocean is 'decay' as in Eq. (2).

3. Results

3.1. Major features of observed dissolved Fe and δ^{56}Fe along the section

Surface ocean δ^{56}Fe varies greatly across the section, with values ranging from about −1‰ above the continental shelf to values as high as +1‰ in the middle of the transect. Low δ^{56}Fe over the shelf probably represents the input of isotopically light Fe from reducing sediments, as seen in profiles above the shelf (Figs. 1, 2) and as previously reported by Chever et al. (2015). At stations in the western portion of the transect (Stns. 20 to 30) δ^{56}Fe decreases in the upper few hundred meters, suggesting that biological activity preferentially removes isotopically heavy Fe. A similar biological removal of heavier isotopes has been observed in the North Atlantic and Southern Ocean, although the mechanism by which this occurs is not known (Conway and John, 2014; Ellwood et al., 2015). A small subsurface tongue of higher δ^{56}Fe waters appear in the eastern portion of the transect (Stns. 5–11) between roughly 100 m to 500 m, in the core of the OMZ (Figs. 1, 2). These higher δ^{56}Fe values could be attributed to the release of isotopically heavy Fe from the sediments due to quantitative Fe dissolution and/or precipitation of isotopically light sulfides within sediment porewaters, both of which there is evidence for along the Peru Margin (Scholz et al., 2014a; Scholz et al., 2014b). However, measured δ^{56}Fe near the sediments is much lower than further from shore, suggesting this is not the case. Alternatively, the heavy dissolved δ^{56}Fe could be the result of the precipitation or particle adsorption of isotopically light Fe in the water column, consistent with observations that particulate δ^{56}Fe is isotopically lighter than the dissolved phase at these depths (Marsay et al., n.d.), and with the active redox cycling of Fe between the dissolved and particulate phases within the OMZ (Heller et al., 2017; Scholz et al., 2016).

The deep ocean is isotopically heavy compared to average continental material (which is ~+0.1‰) at most depths in the western portion of the transect (Stns. 23 to 32) and in the deepest waters (> 3000 m) in the eastern portion of the transect (Stns. 11 to 21). Here, dissolved δ^{56}Fe is generally +0.4 to +0.7‰. These slightly heavy δ^{56}Fe values probably reflect non-reductive input of lithogenic Fe, which has been previously observed in the North Atlantic where the lithogenic phases are dominated by dust (Conway and John, 2014) and in the Southern Ocean where lithogenic phases are more likely to include margin sediments (Abadie et al., 2017).

Finally, there is a plume of Fe emanating from the Peru Margin with low δ^{56}Fe and maximum Fe concentrations between roughly 1000 m to 3000 m. Concentrations are highest near the margin, with elevated Fe (dissolved Fe > 1 nM) persisting roughly 1000 km offshore at Stn 9. Identifiably low δ^{56}Fe waters (δ^{56}Fe < +0.2‰) persist nearly 4000 km offshore to Stn 23. A similar feature was observed near the Mauritanian margin on the US GEOTRACES NAZT (GA03) transect, though the feature was less extensive (~500 km offshore) and the lowest δ^{56}Fe values observed were less negative (the lowest were ~0‰) (Conway and John, 2014). This plume of isotopically light dissolved Fe has a similar spatial distribution to a plume of isotopically light ligand-leachable particulate Fe (Marsay et al., n.d.) (Fig. 3), suggesting possible interaction between particulate and dissolved phases.

The observed high Fe concentrations near the Peru margin are broadly consistent with the release of Fe from the margin, however the specific depth distribution of Fe is surprising. We will devote the remainder of this section to exploring the possible origins of this feature.

3.2. Fe sources and cycling near the Peru margin

Common understanding of the marine Fe cycle suggests that, near continental margins, dissolved Fe concentrations should have a maximum somewhere in the upper ocean (~100 to 1000 m). This is because Fe supply from reducing sediments is generally proportional to the delivery of organic carbon to those sediments (Elrod et al., 2004; Pakhomova et al., 2007), and the flux of organic carbon on the Peru Margin attenuates rapidly over depth (Dale et al., 2015). The input of Fe from oxic sediments occurs more broadly throughout the oceans, and might therefore have greatest impact on Fe concentrations in areas of restricted circulation such as ocean trenches and in the abyssal plains, where Fe is trapped near sediments by sluggish mixing. Nevertheless, in margins dominated by reducing sediments, the largest Fe concentrations should be expected over the shelves and upper slope regions (< 1000 m) where carbon fluxes to the seafloor are largest.

Both simple and complex models of Fe support this view. In our 'source-only' model configuration, the two most important sources of dissolved Fe, organic matter remineralization and dissolved Fe release from reducing sediments, lead to maximum concentrations of Fe in the upper ~200 m (Fig. 4). State-of-the-art models such as PISCES which include a strong source of Fe from reducing sediments tend to produce a Fe maximum in the upper ~1000 m near the Peru margin, while others such as BEC show a broad maximum of Fe near the margin but still no plume in the 1000–3000 m depth range (Fig. 5) (Moore and Braucher, 2008; Tagliabue et al., 2016). Indeed, of 13 models compiled in a recent multi-model intercomparison, none predicted a sedimentary plume of Fe in the 1000–3000 m depth interval in the EPZT transect (Tagliabue et al., 2016).

In contrast to theoretical predictions and observations from the North Atlantic, the main plume of Fe next to the Peru margin occurs most strongly at depths of 1000–3000 m. Close to the sediments, the highest individual Fe concentrations occur just above the continental shelf at Stn 2, 3, and 4 (Fig. 2). By the first off-shelf station (Stn 5), however, high Fe concentrations are no longer observed near the surface and the highest Fe concentrations are clearly observed below 1000 m. While there is variability in Fe concentrations both with depth and distance along the transect, two distinctive features are clear; there is a plume of elevated [Fe] between 1000 m and 3000 m close to the shelf, and isotopically light δ^{56}Fe propagates westward from the shelf with the lowest δ^{56}Fe values observed near the shelf between roughly 1000 m to 3000 m. Below, we differentiate between an "upper-slope" region where offshore Fe concentrations are lower (100–1000 m) and a "mid-slope" region where Fe concentrations are relatively higher (1000–3000 m).

4. Discussion

We consider four reasons why Fe concentrations might be higher at mid-slope depths, 1) the flux of Fe directly from sediments may be greater from the mid-slope compared to upper-slope sediments, 2) the plume does not reflect local dissolved Fe sources, but is instead circulated from a remote region of benthic inputs 3) Fe delivered from mid-slope sediments may be more 'persistent' (more slowly scavenged) than Fe from the upper-slope, or 4) Fe flux from the sediments may be greater from the upper-slope but Fe is subsequently transported to the mid-slope depths by reversible scavenging onto sinking particles (Fig. 6). These hypotheses were tested using the two configurations of our idealized Fe model and data from the transect.

4.1. Is the sedimentary flux of Fe higher on mid-slope?

There is no direct evidence to suggest that sedimentary Fe fluxes are larger from the mid-slope than the upper-slope at the sediment-water interface. Along the California margin observations of Fe fluxes scale with delivery of organic carbon to sediments (Elrod et al., 2004; Pakhomova et al., 2007). Because organic carbon flux attenuates rapidly with depth, this relationship predicts that benthic Fe fluxes should be larger when the seafloor is shallower (Section 3.2). Sediment cores from the Peru Margin support this view. In two studies, sediment cores along the Peru margin down to 1000 m were analyzed to determine sedimentary Fe fluxes based on porewater Fe profiles, and in both cases there was a roughly exponential decrease in Fe fluxes with depth and no

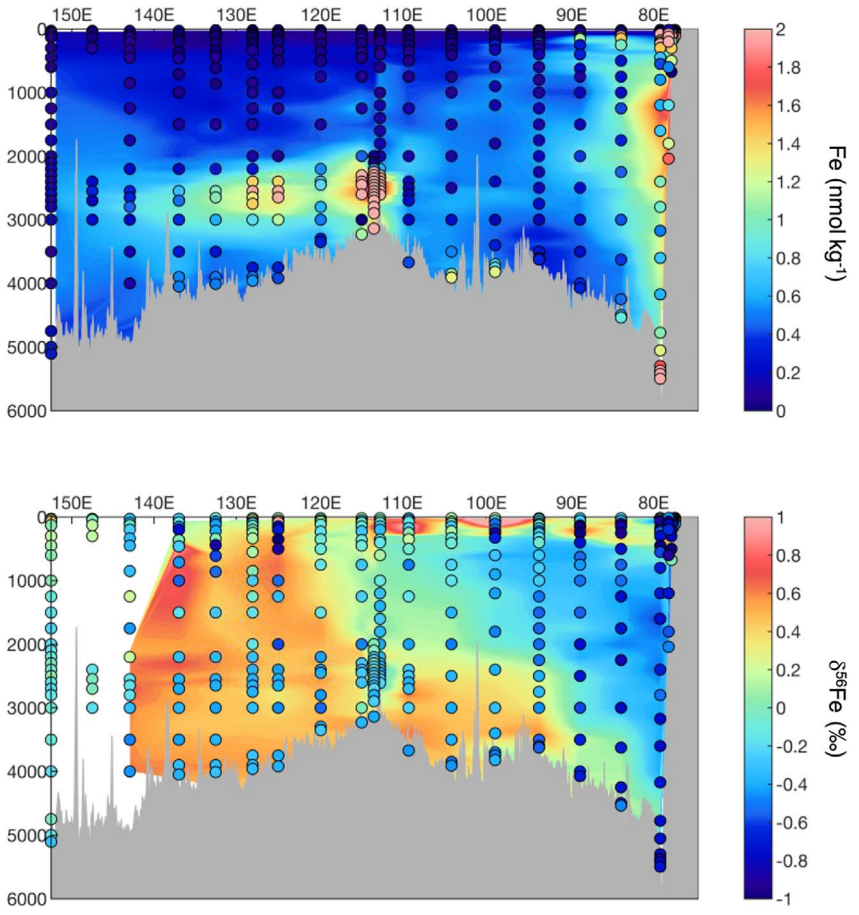

Fig. 3. Particulate ligand-leachable Fe concentrations and δ^{56}Fe from Marsay et al. (n.d.), superimposed upon interpolated dissolved Fe and δ^{56}Fe.

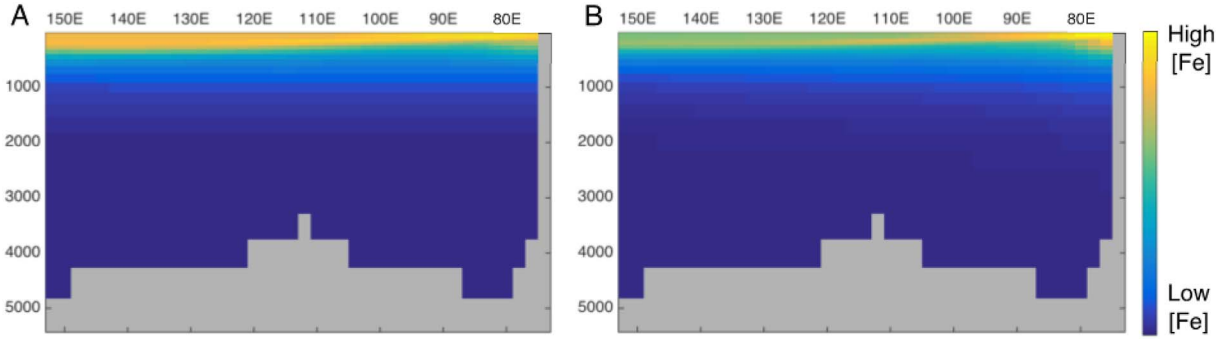

Fig. 4. Model output showing two different source functions for Fe, including biological remineralization assuming a fixed phytoplankton Fe:P stoichiometry (A), and sedimentary remineralization assuming that Fe release is proportional to C respiration in the sediments (B).

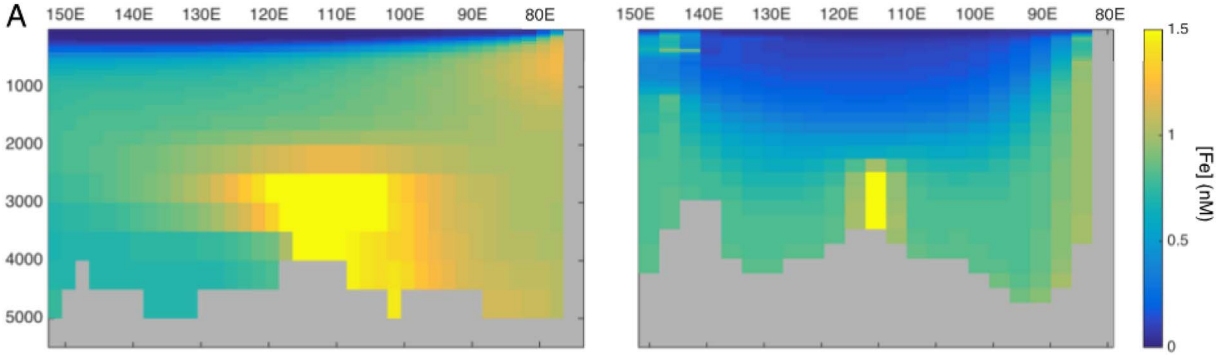

Fig. 5. Current state-of-the-art global biogeochemical models of Fe biogeochemical cycling do not reproduce the observed plume of Fe 1000–3000 m near the Peru margin. Model output from the latitude of the EPZT transect is shown here for PISCES2 (A; Tagliabue et al., 2016) and the BEC (B; Moore and Braucher, 2008).

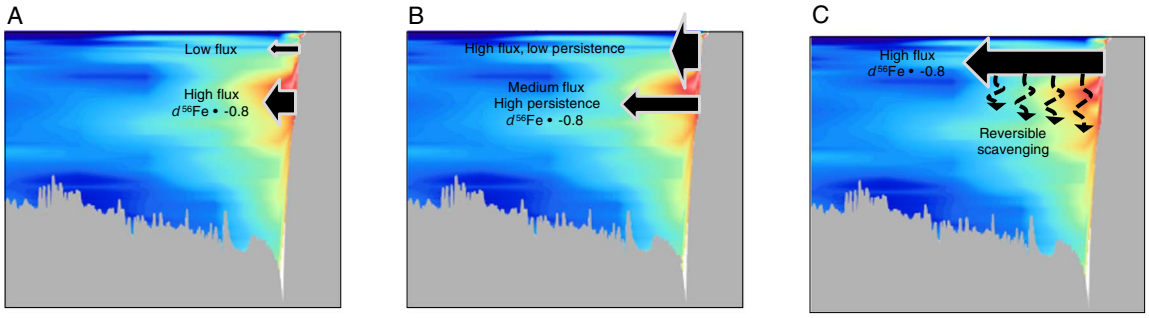

Fig. 6. Possible sources of the mid-slope dissolved Fe plume observed near the Peru margin include a large Fe source between roughly 1000 and 3000 m (A), a source of Fe which is smaller than from the upper shelf but is more persistent (B), or a source of Fe in the upper ocean and reversible scavenging which brings Fe to deeper depths (C). Background is dissolved Fe concentrations as in Fig. 1.

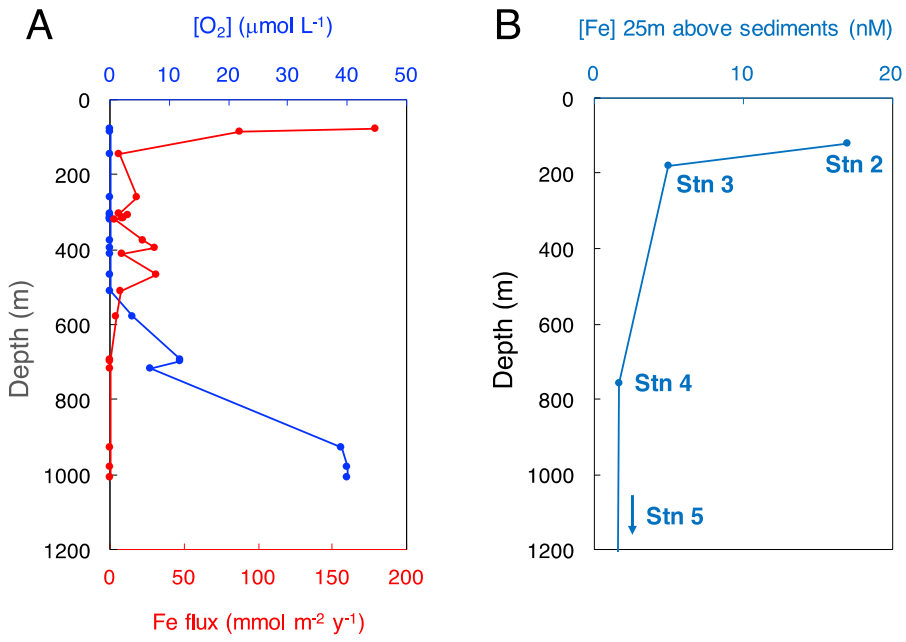

Fig. 7. Flux of Fe from sediments along the Peru margin based on sediment core porewater profiles from Noffke et al. (2012) (similar to more recent data from Scholz et al., 2016) are highest within the upper-slope oxygen minimum zone (A). Higher Fe fluxes correspond to higher water column Fe concentrations, based on our analyses of dissolved Fe interpolated to 25 m above the sediments at stations 2, 3, 4, and 5 (B). High resolution topography of the Peru margin at 12°S from the Global Multi-Resolution Topography database shows the actual slope of the margin at different depths; the dashed line reflects the position of Station 1 (C). Labile (ligand-leachable) Fe and Al profiles from Station 1 show broad maxima in the mid-slope region from 1000 to 3000 m which may point towards sedimentary resuspension at these depths; Fe has another large maximum near the surface attributable to input from reducing sediments, and the increase in Fe and Al below 4500 m may be caused by proximity to the nearby walls of the Peru-Chile trench rather than to increased sedimentary resuspension (D).

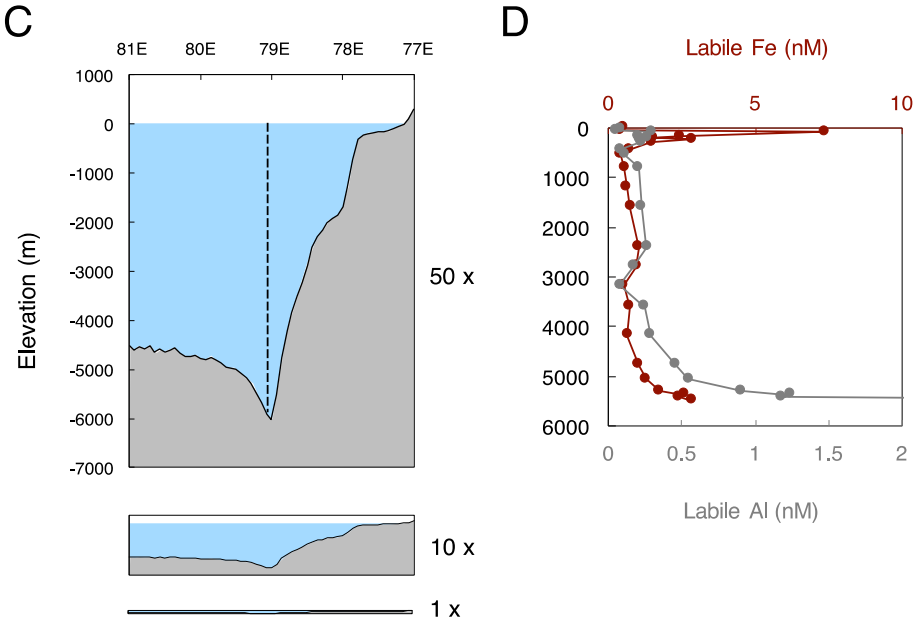

measureable Fe flux below ~700 m (Noffke et al., 2012; Scholz et al., 2016) (Fig. 7). Our data also support a decrease in sedimentary Fe flux with increasing depth. When we linearly interpolate between the bottom two samples to estimate the concentration at 25 m above the sediment-water interface, we find that Fe concentrations decrease for deeper GEOTRACES profiles (Fig. 7). Similarly, concentrations of ligand-leachable (labile) particulate Fe are highest in the upper-slope region (Marsay et al., n.d.) (Fig. 3). Our idealized model shows that when benthic dissolved Fe inputs that are proportional to organic carbon delivery, a shallower plume is produced than the one we observe (Fig. 4a), consistent with more complex biogeochemical models (Moore and Braucher, 2008; Tagliabue et al., 2014). We can therefore rule out this hypothesis.

4.2. Is the plume transported from a remote region?

The Peru Margin is a classic eastern boundary upwelling region. In addition to the upwelling next to the margin driven by Ekman pumping, there are strong meridional subsurface currents, including the northwards flowing Peru Chile Current (PCC) and the southwards-flowing Peru-Chile Countercurrent (PCCC) (Czeschel et al., 2011). Thus, we are motivated to test our Fe input functions within a 3-dimensional model circulation.

Based on our model results, we can also rule the hypothesis that dissolved Fe is released from sediments in remote regions and then circulated towards mid-slope depths off the Peru margin, at least if those remote sources follow simple relationships. Our idealized model simulates benthic dissolved Fe release globally, within in a realistic three-dimensional circulation, and would therefore capture the advection of remotely sourced dissolved Fe. However, our source-only model configuration cannot reproduce the mid-slope plume with either a reducing sediment source pattern (Fig. 4a) or indiscriminate dissolved Fe release from reducing and oxic sediments (Fig. 8a).

Our model includes only simple input functions based on sediment surface area and organic carbon flux, however. It therefore remains possible that there is a unique distal Fe source not represented by our model. For example, high Nd concentrations coupled with radiogenic εNd signatures observed in southwards-flowing mid-depth waters near the Peru margin suggests these waters have interacted with fresh lithogenic material (Grasse et al., 2012), perhaps pointing to a source of highly-reactive minerals from rivers to the north of our study site.

4.3. Is mid-slope Fe delivered in a more persistent form?

Next, we consider the possibility that dissolved Fe is liberated from sediments on the mid-slope in a form that is much more persistent than the fluxes of Fe from reducing sediments on the upper-slope. Fe solubility in seawater is crucially dependent on organic complexation (Rue and Bruland, 1995; Wu and Luther, 1995; Witter and Luther, 1998), so differences in the organic complexation of Fe released from the sediments at different depths could have a large impact on persistence. It is possible that Fe released from the oxic sediments in the middle slope are released along with higher concentrations of organic ligands or with a class of ligands that make this Fe more persistent (less 'scavengeable'). However, we are not aware of experimental data that would directly address the relative persistence of upper-slope and mid-slope Fe. It would also seem to be at odds with the much lower flux of organic carbon to the sediments deeper in the water column.

We tested this hypothesis in the source-only model by simulating the release of persistent dissolved Fe from steep slope sediments, i.e. vertical sediment-ocean gridcell interfaces that are not adjacent to the abyssal plain. This model experiment produces a dissolved Fe plume at similar depths to the observed plume, albeit more confined to the continental margin than observed (Fig. 8b). Mechanistically, such a mid-slope source might result from sediment resuspension in the benthic boundary layer. Internal waves which 'break' on the continental shelf and resuspend sediments increase in energy as the waves are compressed by the slope, so that resuspension might be amplified on the mid-slope (Cacchione and Drake, 1986; Erdem et al., 2016). While our model does not explicitly account for factors such as wave energy, it does suggest that processes that preferentially resuspend sediments on continental slopes could contribute to the observed plume.

Other datasets from the EPZT transect support the hypothesis that there may be an increased resuspension of lithogenic material from mid-slope sediments. Such observational evidence includes higher concentration of small size-fraction lithogenic particulate material at the mid-slope depths of Stns.1 and 5 (Lam et al., n.d.), higher concentrations of ^{228}Ra, which is formed during radioactive decay of lithogenic material, at the mid-slope (Sanial et al., 2017), and higher concentrations of ligand-leachable Fe and Al at the mid-slope (Marsay et al., n.d.; Fig. 7). While the highest concentrations of ligand-leachable Fe were found at upper-slope depths at Stn. 1, there does appear to be a second maximum at mid-slope depths. These three datasets support the hypothesis that the mid-slope Fe maximum may be due to release of Fe from resuspended particles, in a form which is very persistent and can remain dissolved even as it travels thousands of kilometers from the margin.

However, the dissolved δ^{56}Fe data is not necessarily what we would expect in this case. Iron released from oxic sediments typically has δ^{56}Fe similar to, or slightly heavier than, bulk continental values of roughly + 0.1‰ (Beard et al., 2003; Poitrasson, 2006). Oxic sedimentary Fe inputs near + 0.1‰ have been observed in the equatorial western Pacific (Radic et al., 2011), eastern South Atlantic (Homoky et al., 2013), and western North Atlantic (Conway and John, 2014). In this plume, however, we observe δ^{56}Fe values of ~0 to − 1.5‰. Thus, if there is a mid-slope input of persistent Fe, the sediments here must have a different δ^{56}Fe fingerprint than in all of these other locations.

One possible mechanism by which these sediments could have obtained an unusual δ^{56}Fe fingerprint is if they contain high levels of Fe that originated as isotopically light Fe released from upper-slope sediments, precipitated, and then traveled to the mid-slope in benthic boundary flows. However, this is somewhat at odds with previous observations of the 'open-marine iron shuttle' along the Peru Margin (Scholz et al., 2014a). Scholz et al. observed that core-top sedimentary δ^{56}Fe increases with depth along the Peru Margin, to values of about + 0.3‰ below the OMZ. This value is slightly higher than the crustal lithogenic background value of + 0.1‰, suggesting input of isotopically heavier particulate Fe from above. Additionally, Scholz et al. find by mass balance that accumulation of sedimentary Fe just below the OMZ is much less than the loss of sedimentary Fe within OMZ sediments, suggesting that light δ^{56}Fe is transported offshore in the dissolved phase, rather than being transported to sediments below the OMZ.

4.4. Is Fe from the upper-slope transported downwards by reversible scavenging?

Finally, we consider the possibility that more Fe is released from sediments on the upper slope, but that this Fe is subsequently carried down through the water column to the depths of the mid-slope plume on sinking particles. Because the concentration of organic particles decreases strongly over depth, sinking particles can be a sink for dissolved Fe in the upper water column where adsorption exceeds desorption. Deeper in the water column, where attenuation of the particle flux results in net desorption, Fe is released back into the dissolved phase (e.g. Boyd and Ellwood, 2010).

Two simple models were constructed in order to test this hypothesis (Fig. 8c, d). With the first model, which includes input of Fe from reducing sediments and irreversible scavenging of Fe onto sinking particulate organic carbon (POC), we were not able to reproduce a mid-slope plume regardless of the value of $k_{irreversible}$. Increasing $k_{irreversible}$ up to about 1 mM POC^{-1} nM Fe^{-1} caused the Fe plume to become slightly

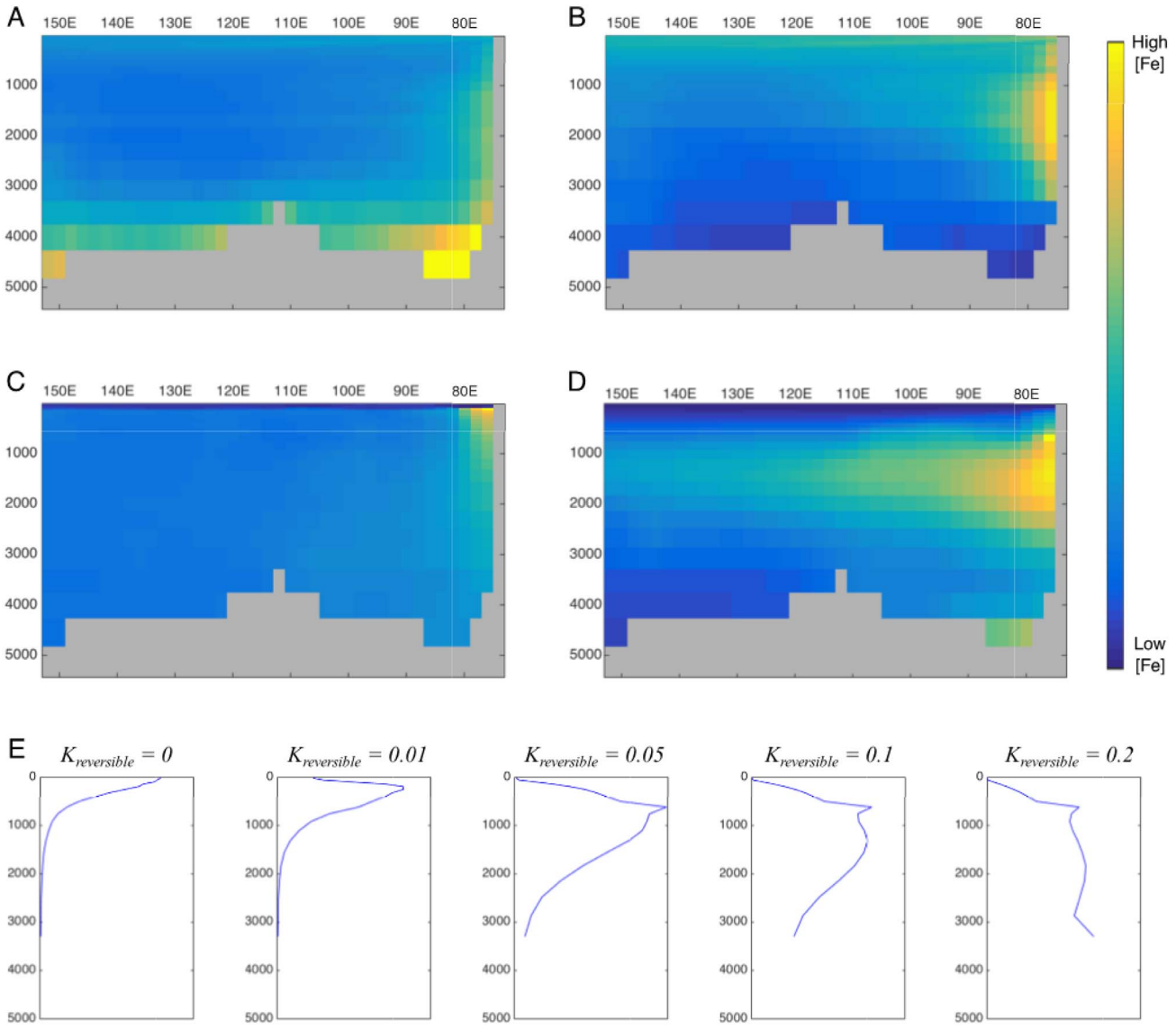

Fig. 8. Simple models which seek to reproduce a plume of Fe at mid-slope depths (1000–3000 m). With input proportional to sediment surface area for every vertical grid-cell face, a plume is not produced (A), though when input is included only from the sides of grid-cells which do not also border the bottom, a mid-slope plume is produced (B). With supply of Fe from reducing sediments and irreversible scavenging to POC, a mid-slope plume cannot be reproduced (C). Using supply of Fe from reducing sediments and reversible scavenging onto sinking POC with a $K_{reversible}$ of 0.1 (mmol C m^{-3})$^{-1}$ produces a mid-slope Fe plume similar to observations (D). Model profiles of Fe concentrations next to the margin demonstrate the effect of changing $K_{reversible}$ on plume depth and plume shape (E).

deeper, but further increases in $k_{irreversible}$ above 1 did not change the depth distribution of the Fe plume. In the second model, we found that increasing $K_{reversible}$ led to a deepening of the Fe plume. Applying a $K_{reversible}$ of 0.1 (mmol C m^{-3})$^{-1}$ produced a mid-slope plume of Fe similar to observations. Further increases in $K_{reversible}$ led to both a broadening and deepening of the plume (Fig. 8).

In situ measurements of the $K_{reversible}$ for Fe in seawater are not available, but we can check whether this value is unrealistically high using data on POC and labile particulate Fe concentrations from the EPZT. Using small size fraction POC concentrations from Stn 1 (Lam et al., n.d.) and dissolved Fe concentrations from our data (interpolated to the same depths as the particulate samples), and a $K_{reversible}$ of 0.1 (mmol C m^{-3})$^{-1}$, we calculate that the average concentration of reversibly scavenged Fe would be roughly 10–100 pM compared to observed 'ligand-leachable' Fe concentrations of 1–10 nM (Fig. 9) (Marsay et al., n.d.). The ligand-leachable pool probably contains many Fe phases that do not readily exchange with the dissolved phase such as the inside of Fe oxyhydroxide minerals and Fe tightly bound in degrading organic material. But if even a few percent of the ligand-leachable pool was reversibly scavenged Fe, it could account for the mid-slope Fe plume. Another factor not testable with this model is the role of alternative iron carrier phases. Our model represents reversible scavenging by POC, but this may only make up around a quarter of the total particle mass (Lam et al., n.d.). Understanding iron scavenging onto calcite and/or biogenic silica, which may have longer remineralization length scales, would be important to appraise in future work.

This hypothesis is more consistent with δ^{56}Fe data. Water column dissolved δ^{56}Fe flux from the upper-slope region is mostly in the range of -1.5‰ to 0‰ in both this work and the work of Chever et al. (2015). The long term δ^{56}Fe flux of -0.53 ± 0.15‰ calculated from sedimentary analyses is also consistent with an isotopically light δ^{56}Fe source from the upper-slope (Scholz et al., 2014a). Both datasets are similar to the dissolved δ^{56}Fe observed within the mid-slope plume. The δ^{56}Fe of the ligand-leachable pool falls in a similar range (Marsay et al., n.d.), suggesting that it could be reversibly exchanging with the dissolved phase (Fig. 3). Fe isotope data are therefore more consistent with

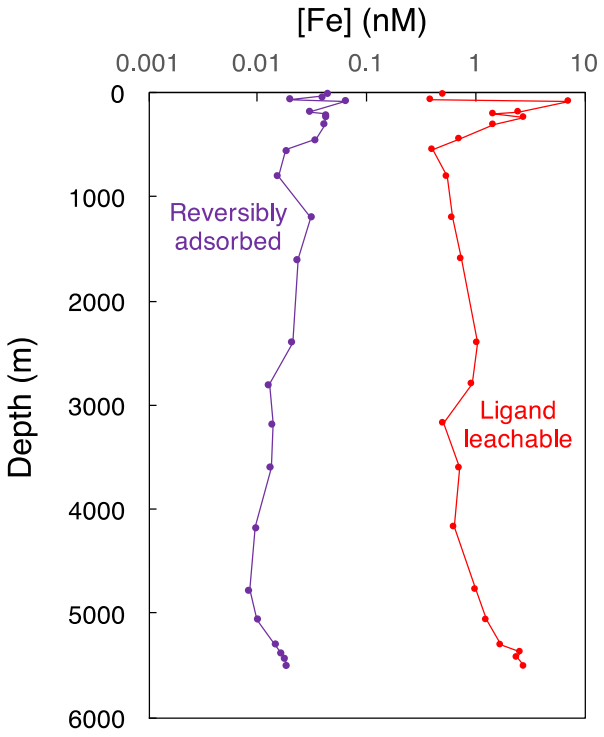

Fig. 9. The concentration of reversibly adsorbed Fe is calculated from the observed concentrations of POC (Lam et al., 2017), dissolved Fe concentrations presented here, and a $K_{reversible}$ of 0.1. Observations of ligand-leachable Fe are taken from Marsay et al. (n.d.). < 10% of the labile (ligand-leachable) Fe would have to be reversibly adsorbed to account for the higher dissolved Fe observed near the mid-slope according to our simple reversible scavenging model.

a reversible scavenging mechanism than with a mid-slope source from dissolution of oxic sediments, though we cannot rule out either hypothesis, or even a combination of both processes.

5. Conclusions and perspectives for future work

The observation of a mid-slope plume of dissolved Fe emanating from the Peru margin is a particularly surprising result of the GP16 transect. While our data are not sufficient to determine the mechanism that produces this feature, its persistence thousands of kilometers from the margin suggests that it reflects a process of global importance to Fe biogeochemical cycling. Furthermore, this feature is not easily explained by current conceptual or numerical models of the global Fe cycle. We therefore suggest that better understanding the origin of the Peru margin mid-slope Fe plume is important to advance our understanding of the global Fe cycle. We put forward three broad questions to help guide future research: 1) What is the mechanism that leads to a mid-slope plume of ^{228}Ra and other lithogenic tracers near the Peru margin, and is it the same mechanism that causes the dissolved Fe plume?; 2) What is the chemical form (speciation) of Fe released from resuspended oxic sediments along the Peru margin, and is it a more persistent form than Fe released from reducing sediments?; 3) Is Fe reversibly scavenged onto sinking particles in the ocean, and if so what is the distribution coefficient ($K_{reversible}$) for different types of natural particles?

Answering these questions will likely require new observations and experiments, combined with modeling efforts to formalize and synthesize our understanding of benthic Fe sources. In particular, the modeling presented here is just a first step towards understanding the possible role of reversible scavenging in the global Fe cycle. While it is intriguing to see that our simple representations of reversible scavenging and margin input can produce a mid-slope plume of Fe, it is important to note that we do not assess the role of many other processes that are considered in more sophisticated models. In models such as BEC and PISCES, scavenging is parameterized in more realistic ways, for example by specifying that only non-ligand bound Fe (Fe′) can be scavenged, and allowing scavenged Fe to be released back to the dissolved phase as particles remineralize (regenerative scavenging) or representing the role of colloidal pumping and multiple carrier phases. Fe input from resuspended sediments can be more realistically modeled by explicitly parameterizing the effects of wave energy and topographical slope on Fe input. Full iron-carbon cycle models also contain many additional processes not represented here, such as biological uptake and recycling of iron, and dynamic representations of ligand chemistry, which may change the effects of reversible scavenging or oxic sedimentary input. In this regard, models that represent the interactions between Fe sources, sinks, and internal cycling in a complex manner can make a more general assessment of the role of the processes highlighted here.

Acknowledgements

Thanks to the captain and crew of the R/V Thomas Thompson, GP16 chief scientists J. Moffett and C. German, and especially to the sampling team who collected all of our dissolved samples at sea including Claire Till, Cheryl Zurbrick, Geoffrey Smith, and Greg Cutter, and to Daniel Ohnemus and the rest of the pump sampling team. This work was supported by NSF Chemical Oceanography grants 1334029 and 1235150 and a grant from the Simons Foundation (SCOPE Award 329108) to John.

References

Abadie, C., Lacan, F., Radic, A., Pradoux, C., Poitrasson, F., 2017. Iron isotopes reveal distinct dissolved iron sources and pathways in the intermediate versus deep Southern Ocean. Proc. Natl. Acad. Sci. 114, 858–863.
Archer, D.E., Johnson, K., 2000. A Model of the iron cycle in the ocean. Global Biogeochem. Cycles 14, 269–279.
Bacon, M.P., Anderson, R.F., 1982. Distribution of Thorium isotopes between dissolved and particulate forms in the deep-sea. J. Geophys. Res. Atmos. 87, 2045–2056.
Beard, B.L., Johnson, C.M., Von Damm, K.L., Poulson, R.L., 2003. Iron isotope constraints on Fe cycling and mass balance in oxygenated Earth oceans. Geology 31, 629–632.
Boiteau, R.M., Fitzsimmons, J.N., Repeta, D.J., Boyle, E.A., 2013. Detection of iron ligands in seawater and marine cyanobacteria cultures by high-performance liquid chromatography–inductively coupled plasma-mass spectrometry. Anal. Chem. 85, 4357–4362.
Boyd, P.W., Ellwood, M.J., 2010. The biogeochemical cycle of iron in the ocean. Nat. Geosci. 3, 675–682.
Cacchione, D.A., Drake, D.E., 1986. Nepheloid layers and internal waves over continental shelves and slopes. Geo-Mar. Lett. 6, 147–152.
Chever, F., Rouxel, O.J., Croot, P.L., Ponzevera, E., Wuttig, K., Auro, M., 2015. Total dissolvable and dissolved iron isotopes in the water column of the Peru upwelling regime. Geochim. Cosmochim. Acta 162, 66–82.
Conway, T.M., John, S.G., 2014. Quantification of dissolved iron sources to the North Atlantic Ocean. Nature 511, 212–215.
Conway, T.M., Rosenberg, A.D., Adkins, J.F., John, S.G., 2013. A new method for precise determination of iron, zinc and cadmium stable isotope ratios in seawater by double-spike mass spectrometry. Anal. Chim. Acta 793, 44–52.
Cutter, G.A., Bruland, K.W., 2012. Rapid and noncontaminating sampling system for trace elements in global ocean surveys. Limnology and Oceanography-Methods 10, 425–436.
Czeschel, R., Stramma, L., Schwarzkopf, F.U., Giese, B.S., Funk, A., Karstensen, J., 2011. Middepth circulation of the eastern tropical South Pacific and its link to the oxygen minimum zone. J. Geophys. Res. Ocean. 116.
Dale, A.W., Sommer, S., Lomnitz, U., Montes, I., Treude, T., Liebetrau, V., Gier, J., Hensen, C., Dengler, M., Stolpovsky, K., Bryant, L.D., Wallmann, K., 2015. Organic carbon production, mineralisation and preservation on the Peruvian margin. Biogeosciences 12, 1537–1559.
DeVries, T., 2014. The oceanic anthropogenic CO_2 sink: storage, air-sea fluxes, and transports over the industrial era. Glob. Biogeochem. Cycles 28, 631–647.
DeVries, T., Liang, J.-H., Deutsch, C., 2014. A mechanistic particle flux model applied to the oceanic phosphorus cycle. Biogeosciences 11, 5381–5398.
Ellwood, M.J., Hutchins, D.A., Lohan, M.C., Milne, A., Nasemann, P., Nodder, S.D., Sander, S.G., Strzepek, R., Wilhelm, S.W., Boyd, P.W., 2015. Iron stable isotopes track pelagic iron cycling during a subtropical phytoplankton bloom. Proceedings of the National Academy of Sciences 112, E15–E20.
Elrod, V.A., Berelson, W.M., Coale, K.H., Johnson, K.S., 2004. The flux of iron from continental shelf sediments: a missing source for global budgets. Geophys. Res. Lett. 31.

Erdem, Z., Schönfeld, J., Glock, N., Dengler, M., Mosch, T., Sommer, S., Elger, J., Eisenhauer, A., 2016. Peruvian sediments as recorders of an evolving hiatus for the last 22 thousand years. Quat. Sci. Rev. 137, 1–14.

Fitzsimmons, J.N., Conway, T.M., Lee, J.-M., Kayser, R., Thyng, K.M., John, S.G., Boyle, E.A., 2016. Dissolved iron and iron isotopes in the southeastern Pacific Ocean. Glob. Biogeochem. Cycles 30, 1372–1395.

Fitzsimmons, J.N., John, S.G., Marsay, C.M., Hoffman, C.L., Nicholas, S.L., Toner, B.M., German, C.R., Sherrell, R.M., 2017. Persistent iron in a distal hydrothermal plume supported by dissolved-particulate exchange. Nat. Geosci. 10, 195–201.

Grasse, P., Stichel, T., Stumpf, R., Stramma, L., Frank, M., 2012. The distribution of neodymium isotopes and concentrations in the Eastern Equatorial Pacific: water mass advection versus particle exchange. Earth Planet. Sci. Lett. 353–354, 198–207.

Guidi, L., Gorsky, G., Claustre, H., Miquel, J.C., Picheral, M., Stemmann, L., 2008. Distribution and fluxes of aggregates > 100 μm in the upper kilometer of the South-Eastern Pacific. Biogeosciences 5, 1361–1372.

Heller, M.I., Lam, P.J., Moffett, J.W., Till, C.P., Lee, J.-M., Toner, B.M., Marcus, M.A., 2017. Accumulation of Fe oxyhydroxides in the Peruvian oxygen deficient zone implies non-oxygen dependent Fe oxidation. Geochim. Cosmochim. Acta. http://dx.doi.org/10.1016/j.gca.2017.05.019.

Homoky, W.B., John, S.G., Conway, T.M., Mills, R.A., 2013. Distinct iron isotopic signatures and supply from marine sediment dissolution. Nat. Commun. 4, 2143.

John, S.G., Mendez, J., Moffett, J., Adkins, J.F., 2012. The flux of iron and iron isotopes from San Pedro Basin sediments. Geochim. Cosmochim. Acta 93, 14–29.

Khatiwala, S., 2007. A computational framework for simulation of biogeochemical tracers in the ocean. Global Biogeochem. Cycles 21. http://dx.doi.org/10.1029/2007GB002923.

Lam, P.J., Lee, J.-M., and Heller, M.I. (n.d.) Size-fractionated distributions of suspended particle concentration and major phase composition from the U.S. GEOTRACES Eastern Pacific Zonal Transect (GP16). Mar. Chem.

Marsay, C.M., Lam, P.J., Heller, M.I., Lee, J.-M., and John, S.G. (n.d.) Distribution and isotopic signature of ligand-leachable particulate iron along the GEOTRACES GP16 East Pacific Zonal Transect. Marine Chemistry, (submitted).

Moore, J.K., Braucher, O., 2008. Sedimentary and mineral dust sources of dissolved iron to the world ocean. Biogeosciences 5, 631–656.

Moore, J.K., Doney, S.C., 2007. Iron availability limits the ocean nitrogen inventory stabilizing feedbacks between marine denitrification and nitrogen fixation (Global Biogeochem. Cycles). 21. http://dx.doi.org/10.1029/2006GB002762.

Moore, J.K., Doney, S.C., Lindsay, K., 2004. Upper ocean ecosystem dynamics and iron cycling in a global three-dimensional model. Glob. Biogeochem. Cycles 18.

Noffke, A., Hensen, C., Sommer, S., Scholz, F., Bohlen, L., Mosch, T., Graco, M., Wallmann, K., 2012. Benthic iron and phosphorus fluxes across the Peruvian oxygen minimum zone. Limnol. Oceanogr. 57, 851–867.

Pakhomova, S.V., Hall, P.O.J., Kononets, M.Y., Rozanov, A.G., Tengberg, A., Vershinin, A.V., 2007. Fluxes of iron and manganese across the sediment–water interface under various redox conditions. Mar. Chem. 107, 319–331.

Parekh, P., Follows, M.J., Boyle, E., 2004. Modeling the global ocean iron cycle. Glob. Biogeochem. Cycles 18.

Peters, B.D., Casciotti, K., Jenkins, W.J., Swift, J.H., German, C.R., Moffett, J.W., Cutter, G.A., Brzezinski, M.A., 2017. Water mass analysis of the 2013 US GEOTRACES Eastern Pacific Zonal Transect. Mar. Chem (in press).

Poitrasson, F., 2006. On the iron isotope homogeneity level of the continental crust. Chem. Geol. 235, 195–200.

Radic, A., Lacan, F., Murray, J.W., 2011. Iron isotopes in the seawater of the equatorial Pacific Ocean: new constraints for the oceanic iron cycle. Earth Planet. Sci. Lett. 306, 1–10.

Resing, J.A., Sedwick, P.N., German, C.R., Jenkins, W.J., Moffett, J.W., Sohst, B.M., Tagliabue, A., 2015. Basin-scale transport of hydrothermal dissolved metals across the South Pacific Ocean. Nature 523, 200–203.

Rue, E.L., Bruland, K.W., 1995. Complexation of iron(III) by natural organic ligands in the Central North Pacific as determined by a new competitive ligand equilibration adsorptive cathodic stripping voltammetric method. Mar. Chem. 50, 117–138.

Sanial, V., Kipp, L.E., Henderson, P., van Beek, P., Reyss, J.-L., Hammond, D.E., Hawco, N., Saito, M.A., Resing, J.A., Sedwick, P.N., et al., 2017. Radium-228 as a tracer of dissolved trace element inputs from the Peruvian continental margin. Mar. Chem. http://dx.doi.org/10.1016/j.marchem.2017.05.008.

Scholz, F., Severmann, S., McManus, J., Hensen, C., 2014a. Beyond the Black Sea paradigm: the sedimentary fingerprint of an open-marine iron shuttle. Geochim. Cosmochim. Acta 127, 368–380.

Scholz, F., Severmann, S., McManus, J., Noffke, A., Lomnitz, U., Hensen, C., 2014b. On the isotope composition of reactive iron in marine sediments: redox shuttle versus early diagenesis. Chem. Geol. 389, 48–59.

Scholz, F., Löscher, C.R., Fiskal, A., Sommer, S., Hensen, C., Lomnitz, U., Wuttig, K., Göttlicher, J., Kossel, E., Steininger, R., Canfield, D.E., 2016. Nitrate-dependent iron oxidation limits iron transport in anoxic ocean regions. Earth Planet. Sci. Lett. 454, 272–281.

Severmann, S., Johnson, C.M., Beard, B.L., McManus, J., 2006. The effect of early diagenesis on the Fe isotope compositions of porewaters and authigenic minerals in continental margin sediments. Geochim. Cosmochim. Acta 70, 2006–2022.

Severmann, S., McManus, J., Berelson, W.M., Hammond, D.E., 2010. The continental shelf benthic iron flux and its isotope composition. Geochim. Cosmochim. Acta 74, 3984–4004.

Tagliabue, A., Aumont, O., Bopp, L., 2014. The impact of different external sources of iron on the global carbon cycle. Geophys. Res. Lett. 41, 920–926.

Tagliabue, A., Aumont, O., DeAth, R., Dunne, J.P., Dutkiewicz, S., Galbraith, E., Misumi, K., Moore, J.K., Ridgwell, A., Sherman, E., et al., 2016. How well do global ocean biogeochemistry models simulate dissolved iron distributions? Global Biogeochemical Cycles 30, 149–174.

Tagliabue, A., Bowie, A.R., Boyd, P.W., Buck, K., Johnson, K.S., Saito, M.A., 2017. The integral role of iron in ocean biogeochemistry. Nature 543, 51–59.

Vedamati, J., Goepfert, T., Moffett, J.W., 2014. Iron speciation in the eastern tropical South Pacific oxygen minimum zone off Peru. Limnol. Oceanogr. 59, 1945–1957.

Witter, A.E., Luther, G.W., 1998. Variation in Fe-organic complexation with depth in the Northwestern Atlantic Ocean as determined using a kinetic approach. Mar. Chem. 62, 241–258.

Wu, J.F., Luther, G.W., 1995. Complexation of Fe(III) by natural organic ligands in the Northwest Atlantic Ocean by a competitive ligand equilibration method and a kinetic approach. Mar. Chem. 50, 159–177.

View publication stats